PNAS RESEARCH ARTICLE | APPLIED PHYSICAL SCIENCES

# Free-electron resonance transition radiation via Brewster randomness

Zheng Gong[a,b], Ruoxi Chen[a,b], Zun Wang[c], Xiangfeng Xi[a,b], Yi Yang[d], Baile Zhang[e,f,1], Hongsheng Chen[a,b,g,h,1], Ido Kaminer[i], and Xiao Lin[a,b,1]

Affiliations are included on p. 7.

Edited by Hui Cao, Yale University, New Haven, CT; received July 3, 2024; accepted December 30, 2024

**Free-electron radiation, such as Cherenkov radiation and transition radiation, can generate light at arbitrary frequencies and is fundamental to diverse applications, ranging from electron microscopy, spectroscopy, lasers, to particle detectors. Generally, the features of free-electron radiation are stochastic when electrons interact with random media. Counterintuitively, here, we reveal a type of free-electron radiation that has both its intensity and directionality invariant to specific sorts of long-range structural randomness. Essentially, this invariance is enabled by the Brewster effect and the judiciously engineered phase coherence condition of emitted light, namely that the light induced by electron's penetration through a layered aperiodic nanostructure is engineered to interfere constructively at the Brewster angle. As such, when each constituent layer with a random thickness fulfills this phase coherence condition, there is always the emergence of free-electron resonance transition radiation at the Brewster angle. At this resonant Brewster angle, we further find that the radiation intensity and directionality could be enhanced by orders of magnitude by readily increasing the interface number. The revealed resonance transition radiation via long-range Brewster randomness may offer a feasible route to explore more enticing photonic applications driven by free electrons, such as light sources at previously unreachable spectral regimes, optical frequency combs, particle detectors, and random lasers.**

free-electron radiation | random media | Brewster effect | resonance transition radiation | random laser

## Significance

Light emission from random media, e.g., free-electron radiation, is widely believed to have stochastic optical features. Here, we break this long-held belief by revealing an exotic type of free-electron radiation that has both its intensity and directionality at a predefined working wavelength invariant to specific sorts of structural randomness, when considering relatively small material losses. Remarkably, this anomalous invariance-to-randomness correspondence could still emerge even in the presence of both long-range and short-range randomness. We further reveal that this surprising resonant phenomenon of light emission essentially arises from the combination of three seemingly disjoint phenomena: Brewster effect, random media, and free-electron radiation. Accordingly, our finding indicates exciting possibilities of reshaping free-electron radiation via random media in a controllable and flexible way.

Free-electron radiation (1–7), as an elementary emission mechanism of light, is of fundamental relevance to many diverse scientific realms, such as nuclear physics and cosmology (8–11). One paradigmatic example is Cherenkov radiation (8, 12–22), which is the characteristic bluish glow of water-cooled nuclear reactors and would emerge when a charged particle (e.g., a swift electron) moves faster than the phase velocity of light in the surrounding matter. Another paradigmatic example of free-electron radiation is transition radiation (23–32), which contributes significantly to the radio emission of the Earth, the Sun, and many interstellar and interplanetary media (33, 34) and occurs whenever a charged particle moves across an optical interface. Up to now, the free-electron radiation has enabled many practical applications, including electron microscopy (35–40), free-electron lasers (41–43), particle detection (44–49), beam diagnostics (50, 51), quantum information processing (19, 52), and medical therapy (53, 54), mainly due to its unique capability to create light emission at arbitrary desired spectral regimes.

Generally, the features of free-electron radiation are random if free electrons interact with random media. The underlying reason is that the random media with either long-range or short-range randomness would give rise to complex yet stochastic multiple scattering of light. On the one hand, it is well known that both short and long-range randomness in photonic structures might create optical scattering and eventual opacity, due to Anderson-localization-type phenomena (55–58). On the other hand, the Debye–Waller effect (59, 60) explains how short-range random fluctuations in periodic structures (e.g., those in atomic crystals caused by thermal motion) could preserve coherence but would cause the attenuation of scattering amplitude, for example, during the diffraction process of X-rays, electrons or neutrons. In short, the occurrence of stochastic scattering of light unavoidably makes the prediction and then the manipulation of free-electron radiation from random media challenging (61–65).

Despite the long research history of free-electron radiation (66–72) and randomness in photonic structures (55–57, 60, 73–75), the investigation of free-electron radiation from random media is still in its infancy and mainly focused on the short-range randomness (76–78). Generally, the short-range randomness, which still preserves the long-range order, does not inhibit the conventional mechanisms of free-electron radiation, since free-electron radiation occurs in a nonlocal fashion (78). Accordingly, the short-range

Author contributions: Z.G. and X.L. designed research; Z.G. performed research; Z.G., R.C., Z.W., X.X., Y.Y., B.Z., H.C., I.K., and X.L. analyzed data; B.Z., H.C., and I.K. supervised the project; and Z.G. and X.L. wrote the paper.

The authors declare no competing interest.

This article is a PNAS Direct Submission.



[1]To whom correspondence may be addressed. Email: blzhang@ntu.edu.sg, hansomchen@zju.edu.cn, or xiaolinzju@zju.edu.cn.

This article contains supporting information online at https://www.pnas.org/lookup/suppl/doi:10.1073/pnas.2413336122/-/DCSupplemental.

Published February 5, 2025.

randomness was found capable to spatially and spectrally shape the free-electron radiation, such as the manipulation of free-electron Smith-Purcell radiation (79–82) via aperiodic nanostructures (76, 77). Till now, there remains an active interest in the role of randomness in free-electron radiation, partly due to the existence of many open scientific questions. Particularly, whether there are specific sorts of structural randomness, especially those with long-range randomness, that could enable some invariant features of free-electron radiation remains elusive.

Here, we reveal an enticing possibility to create some *invariant* features (i.e., the characteristic intensity and directionality of emitted light) of free-electron radiation via *random* media. Remarkably, this invariance-to-randomness correspondence of free-electron radiation would still emerge even in presence of long-range randomness. This finding indicates an exotic randomness-enabled way to significantly improve the performance (e.g., intensity and directionality) of free-electron radiation, for example, by increasing the interface number. The continual exploration of this invariance-to-randomness correspondence might inspire disruptive ways to control light–matter interactions and is of great interdisciplinary interest. As background, the randomness-to-randomness correspondence is indeed universal not only in free-electron radiation and photonics but also in other realms of physics, technology, and even philosophy (58, 83–85).

At the core of this work lies the paradigm to achieve the free-electron resonance transition radiation from random layered aperiodic nanostructures with the aid of Brewster effect. The Brewster effect (30, 86–93), dating back to the pioneering work of Sir David Brewster in the early 1810s, describes a total transmission phenomenon through a dielectric interface under the incidence of *p*-polarized light at the so-called Brewster angle. Recently, it was reported that the Brewster effect can provide a unique route to tailor free-electron radiation, such as the usage of the Brewster effect from stacks of variable one-dimensional photonic crystals to angularly filter the Cherenkov radiation (93) and the usage of the pseudo-Brewster effect from a gain dielectric slab to enhance both the intensity and directionality of transition radiation (30). While these previous studies are limited to the framework of either ordered (30) or locally ordered (93) nanostructures, the intricate interplay between the Brewster effect in aperiodic nanostructures with the long-range randomness and the resonance transition radiation remains unexplored. Essentially, our revealed invariance-to-randomness correspondence for free-electron radiation is achieved by simultaneously enforcing the Brewster effect and a judiciously designed phase coherence condition of emitted light. In other words, the multiple transition radiation created at adjacent interfaces is engineered to interfere constructively at the Brewster angle. Then, if each constituent layer with a random thickness is designed to fulfill this phase coherence condition, we find that there is always the formation of resonance transition radiation at the Brewster angle, whose intensity and directionality are robust to the random variations of each layer thickness. Accordingly, this special sort of structural variation with the long-range randomness is suggested to be termed the Brewster randomness, owing to the fundamental role of Brewster effect. Our revealed Brewster randomness indicates the intriguing potential to reshape free-electron radiation from random media in a controllable and flexible way.

## Results

We begin with the introduction on how to construct the Brewster randomness for free-electron resonance transition radiation. As schematically shown in Fig. 1*A*, the swift electron with a velocity $\overline{v} = \hat{z}v$ perpendicularly penetrates through a layered aperiodic nanostructure composed of alternating dielectrics I and II (94–97). In practice, in order to avoid the inelastic electron scattering, a tiny hole with its center along the trajectory of electron could be drilled inside the designed sample (98, 99). For conceptual brevity, the electron velocity is chosen to have $v < \min\left(c/\sqrt{\varepsilon_{\mathrm{r,I}}}, c/\sqrt{\varepsilon_{\mathrm{r,II}}}\right)$, such that the Cherenkov radiation is fully prohibited, where $c$ is the light speed in vacuum, $\varepsilon_{\mathrm{r,X}}$ is the relative permittivity of dielectric X, and X = I or II. In other words, there is only the emergence of transition radiation in this work, which is purely *p*-polarized.

According to the Brewster effect, the *p*-polarized transition radiation would totally transmit through the adjacent interface between dielectrics I and II in Fig. 1*B*, when it propagates along the Brewster angle $\theta_{\mathrm{B,X}} = \arccos\sqrt{\frac{\varepsilon_{\mathrm{r,X}}}{\varepsilon_{\mathrm{r,I}}+\varepsilon_{\mathrm{r,II}}}}$ inside dielectric X. Enabled by this unique capability of Brewster effect, the phase difference between multiple transition radiation emanating from different optical interfaces at the Brewster angle can be readily calculated by exploiting the geometric optics in Fig. 1 *C* and *D*. To be specific, the phase difference $\Delta\varphi$ between the forward-propagating transition radiation from the interface of $z = z_{j-1}$ and that from the interface of $z = z_j$ at the Brewster angle can be analytically obtained as

$$\Delta\varphi = \omega d_{\mathrm{X}}/v - \pi - k_{z,\mathrm{X}} d_{\mathrm{X}}, \qquad [1]$$

where $k_{z,\mathrm{X}} = \frac{\omega}{c} \cdot \frac{\varepsilon_{\mathrm{r,X}}}{\sqrt{\varepsilon_{\mathrm{r,I}}+\varepsilon_{\mathrm{r,II}}}}$ is the $z$-component wavevector of light propagating along the Brewster angle in dielectric X, $d_{\mathrm{X}} = z_j - z_{j-1}$ is the thickness of the corresponding layer composed of dielectric X, and $\omega$ is the angular frequency.

If the phase coherence condition of $\mathrm{mod}(\Delta\varphi, 2\pi) = 0$ is fulfilled, the multiple transition radiation from different optical interfaces would interfere constructively. As a result, the resonance transition radiation would emerge and manifest itself as plane-like waves propagating along the Brewster angle in the forward vacuum region (i.e., region $N + 1$ in Fig. 1*E*). According to this phase coherence condition, the corresponding layer thickness could be obtained as

$$d_{\mathrm{X}} = \left(2m_{\mathrm{X}} + 1\right) \cdot d_{\mathrm{B,X}}, \qquad [2]$$

$$d_{\mathrm{B,X}} = \frac{\lambda}{2\left(c/v - \varepsilon_{\mathrm{r,X}}/\sqrt{\varepsilon_{\mathrm{r,I}}+\varepsilon_{\mathrm{r,II}}}\right)}, \qquad [3]$$

where $m_{\mathrm{X}} \geq 0$ is a random integer and $\lambda = 2\pi c/\omega$ is the wavelength of light in free space. Once the thickness of each constituent layer is randomly chosen but governed by Eqs. **2** and **3**, the designed layered aperiodic nanostructure has the Brewster randomness. According to Eqs. **2** and **3**, the proposed Brewster randomness belongs to a specific sort of long-range randomness (85), without the consideration of short-range disorders (e.g., those caused by imperfect sample fabrications). Actually, the addition of short-range disorders into the designed layered nanostructure would not inhibit the exotic capability of Brewster randomness in the manipulation of free-electron radiation (*SI Appendix*, Figs. S3–S5). For conceptual demonstration, the discussion below focuses on the Brewster randomness described by Eqs. **2** and **3**.

The validity of Eqs. **2** and **3** can be further verified by analyzing the angular spectral energy density of free-electron radiation from layered nanostructures at a predefined working wavelength of $\lambda = \lambda_0$ (e.g., $\lambda_0 = 500$ nm) in Fig. 2. The angular spectral energy

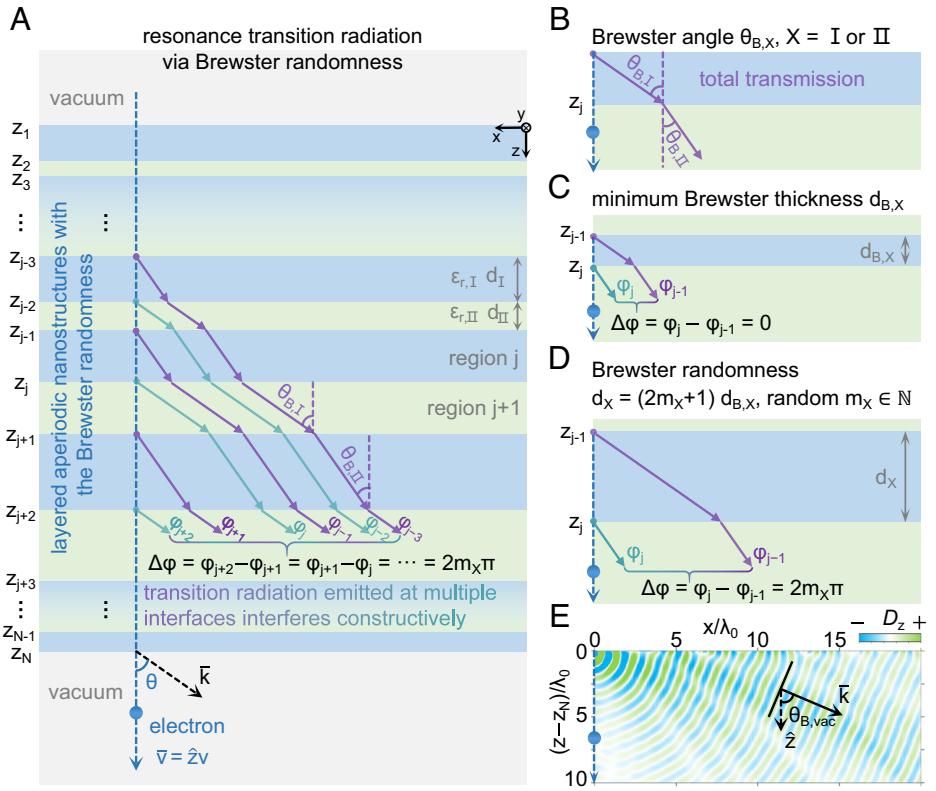


**Fig. 1.** Conceptual demonstration of free-electron resonance transition radiation from a layered aperiodic nanostructure with Brewster randomness. (*A–D*) Structural schematic for the design of layered aperiodic nanostructures. The layered nanostructure in *A* has *N* parallel interfaces and is composed of two alternating dielectrics, namely dielectric I and dielectric II. Each dielectric has a relative permittivity $\epsilon_{r,X}$ and a thickness $d_X$, where X = I or II. If the emitted light propagates at the Brewster angle $\theta_{B,X}$ in dielectric X, as depicted in *B*, it could totally transmit through the adjacent interface between dielectric I and II. Meanwhile, the light emitted from the interface of $z = z_j$ and forward propagating in region *J* has a phase $\varphi_j$ in *C* and *D*, where *j* and *J* are both integers and $J > j$. If the phase coherence condition of $\Delta\varphi = \varphi_j - \varphi_{j-1} = 2m_X\pi$ is fulfilled, all transmitted light at the Brewster angle in region *J* would interfere constructively, where $m_X \geq 0$ is a random interger. If the thickness of each dielectric layer is designed to fulfill this phase coherence condition, the resonance transition radiation could be formed at the Brewster angle. Then, this judiciously engineered layered nanostructure is termed to have the Brewster randomness. For the Brewster randomness, the minimum thickness of dielectric X could be obtained by letting $m_X = 0$ in the phase coherence condition, and it is set to be $d_X = d_{B,X}$ in *C*. When $m_X \neq 0$, we further have $d_X = (2m_X+1)d_{B,X}$ in *D*. (*E*) Field distribution of free-electron resonance transition radiation via the Brewster randomness in region $N+1$. Without further specification, for all the figures in the main text, we set $N = 100$, $\epsilon_{r,I} = 2.1$ [e.g., $SiO_2$ (94)], $\epsilon_{r,II} = 1.4$ [e.g., $ZrO_2$ aerogel (95)], the particle velocity $v = v_0 = 0.3c < \min\left(c/\sqrt{\epsilon_{r,I}}, c/\sqrt{\epsilon_{r,II}}\right)$ to avoid the Cherenkov radiation, the surrounding environment being vacuum, $m_X$ being randomly distributed from 0 to 9, and the working wavelength $\lambda = \lambda_0 = 500$ nm.

density $U(\lambda, \theta)$ in Fig. 2 is derived by extending Ginzburg and Frank's theory of transition radiation (23, 25), where $\theta$ is the radiation angle in the forward vacuum region. For illustration, the thickness of all layers composed of dielectric II is chosen to be the same inside the whole layered nanostructure, such as $d_{II} \equiv d_{B,II}$ in Fig. 2*A*, which already satisfies Eqs. **2** and **3**. Without loss of generality, the thickness of each layer composed of dielectric I in Fig. 2*A* is set to be $d_I = (2\,m_I+1)d_{0,I}$, where $d_{0,I}$ is a fixed constant but $m_I$ is a random integer from the top to the bottom of the layered nanostructure. Under this scenario, only if $d_{0,I}/d_{B,I}$ is an odd integer, the thickness of all layers composed of dielectric I would satisfy Eqs. **2** and **3**, and then, the designed layered nanostructure has the Brewster randomness.

We find that irrespective of the randomness of $m_I$, the resonance transition radiation emerges at $\theta = \theta_{B,vac}$ for $d_{0,I}/d_{B,I} = 1$ in Fig. 2*B*, where the angle $\theta_{B,vac} = \arccos\sqrt{\frac{\epsilon_{r,I}\epsilon_{r,II}}{\epsilon_{r,I}+\epsilon_{r,II}}}$ corresponds to the Brewster angle in the forward vacuum region. More generally, there is the emergence of strong radiation peaks in Fig. 2*C* if $d_{0,I}/d_{B,I}$ is an odd integer, which clearly indicates that the Brewster randomness can always give rise to the resonance transition radiation with high directionality at the Brewster angle. Upon close inspection of Eqs. **2** and **3**, the layer thickness used for the construction of Brewster randomness is also sensitive to the electron velocity, as shown in Fig. 2*D*. In addition, if $d_X/d_{B,X}$ is an even integer, the multiple transition radiation created at adjacent interfaces would interfere destructively, leading to the formation of radiation dips in Fig. 2 *C* and *D* and *SI Appendix*, Fig. S6.

With the knowledge of how to construct the Brewster randomness, Fig. 3 investigates the interaction of free electrons with various Brewster randomness in the $\lambda$-$\theta$ parameter space, which is intrinsically related to the energy–momentum space of emitted light. As governed by Eqs. **2** and **3**, all Brewster randomness in Fig. 3 is designed at a prescribed working wavelength of $\lambda = \lambda_0$ with the usage of $\epsilon_{r,I} = 6.1$ [e.g., $SrTiO_3$ (94)] and $\epsilon_{r,II} = 1$. From the angular spectral energy density, Fig. 3 *A–C* shows that there are a bunch of radiation peaks in the $\lambda$-$\theta$ parameter space, which can be categorized into three types. First, the appearance of most radiation peaks is intrinsically random and generally sensitive to the variation of Brewster randomness (i.e., the random choice of $m_I$ and $m_{II}$ in Eqs. **2** and **3**). Second, when $\lambda \to \lambda_0$ and $\theta \to \theta_{B,vac} = 67.96°$, the appearance of some radiation peaks in Fig. 3 *A–C* becomes relatively insensitive to the variation of Brewster randomness. We further show in *SI Appendix*, Fig. S7 that the emergence range of these radiation peaks in the energy–momentum space of emitted light can be flexibly tailored through the judicious manipulation

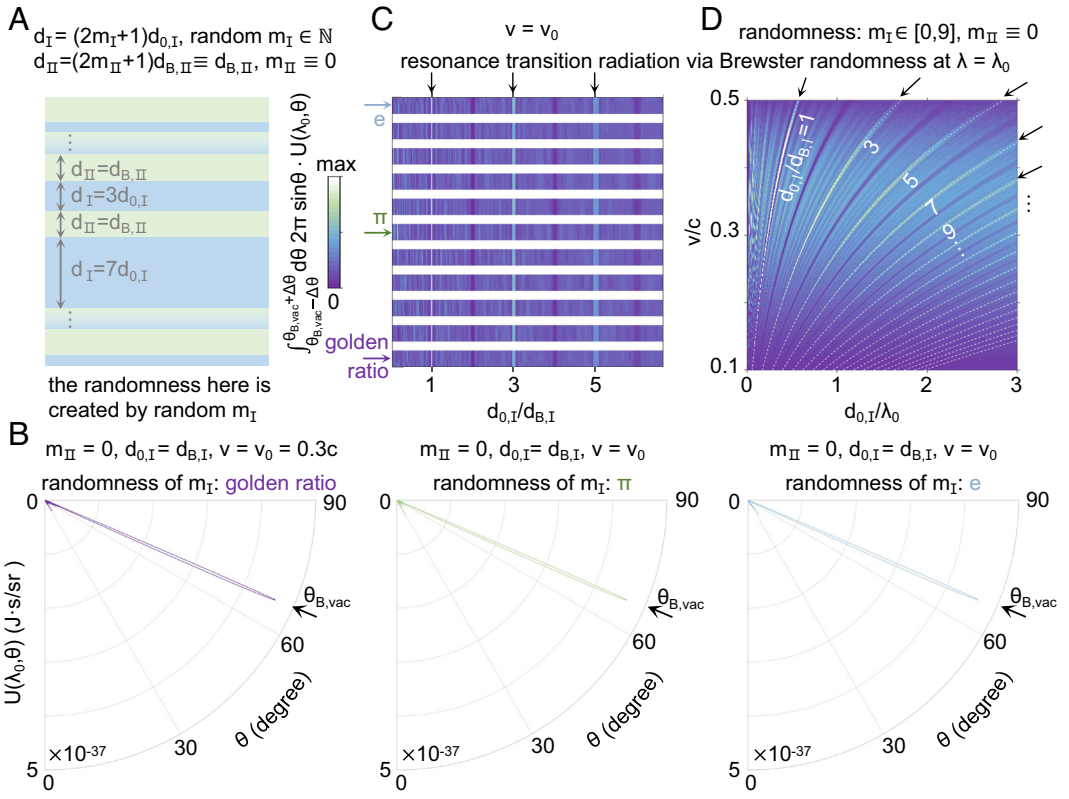


**Fig. 2.** Angular spectral energy density of free-electron resonance transition radiation via Brewster randomness at a predefined working wavelength $\lambda = \lambda_0$ (e.g., $\lambda_0$ = 500 nm in the calculation). For conceptual illustration, here, we use $\epsilon_{r,I} = 2.1$ and $\epsilon_{r,II} = 1.4$. (*A*) Structural schematic of the layered aperiodic nanostructure. The thickness of each layer composed of dielectric II is the same inside the whole structure, namely $d_{II} = d_{B,II}$, and the thickness of the layer composed of dielectric I is $d_I = (2m_I+1)d_{0,I}$, where $d_{0,I}$ is a fixed constant and $m_I$ is a random interger. Then, the designed layered aperiodic nanostructure has the Brewster randomness only if $d_{0,I}/d_{B,I}$ is an odd integer. (*B*) Angular spectral energy density $U(\lambda_0,\theta)$ of free-electron forward radiation into region $N+1$, by letting $d_{0,I}/d_{B,I} = 1$. For layers composed of dielectric I, from the top to the bottom, the choice of $m_I$ follows the decimal expansion of some irrational numbers to test various Brewster randomness, such as the golden ratio $(1+\sqrt{5}/2)$ with $m_I$ = 1, 6, 1, 8... in the *Left* panel, $\pi$ with $m_I$ = 3, 1, 4, 1... in the *Middle* panel, and Euler's number $e$ with $m_I$ = 2, 7, 1, 8.... in the *Right* panel. (*C*) $\int_{\theta_{B,vac}-\Delta\theta}^{\theta_{B,vac}+\Delta\theta} d\theta(2\pi\sin\theta)U(\lambda_0,\theta)$ as a function of $d_{0,I}$ for various randomness of $m_I \in [0,9]$ for cases studied in *B* and other cases with computer-generated randomness, under the scenario of $v = v_0 = 0.3c$ and $\Delta\theta = 5°$. (*D*) $\int_{\theta_{B,vac}-\Delta\theta}^{\theta_{B,vac}+\Delta\theta} d\theta(2\pi\sin\theta)U(\lambda_0,\theta)$ as a function of $d_{0,I}$ and $v$, with computer-generated random integer $m_I \in [0,9]$.

of material dispersion. Third, strictly speaking, only the radiation peak at the special point of ($l_0$,$q_{B,vac}$) in Fig. 3 *A*–*C* is invariant to the variation of Brewster randomness.

To gain a deeper understanding, we extract the dependence of $\lambda_{max}$ on $\theta$ for various Brewster randomness in Fig. 3*D*. This dependence is calculated by using the definition of $U(\lambda_{max}, \theta) = \max[U(\lambda,\theta), \lambda]$ inside a relatively small region, which contains the special point of $(\lambda_0, \theta_{B,vac})$, such as the region with $\lambda/\lambda_0 \in [0.99, 1.01]$ and $\theta \in [64°, 72°]$ in Fig. 3 *A*–*C*. From Fig. 3*D*, there is always a fixed overlapped point at $\lambda_{max} = \lambda_0$ and $\theta = \theta_{B,vac}$. Meanwhile, Fig. 3*E* shows the dependence of $U(\lambda_{max}, \theta)$ on $\theta$. We find that only the value of $U(\lambda_{max}, \theta_{B,vac})$ in Fig. 3*E* would maintain unchanged under the variation of Brewster randomness. When the radiation angle $\theta$ is further away from the Brewster angle $\theta_{B,vac}$, the value of $U(\lambda_{max}, \theta)$ in Fig. 3*E* would become more sensitive to the variation of Brewster randomness.

We now proceed to study the influence of the interface number $N$ on the resonance transition radiation via the Brewster randomness in Fig. 4 *A*–*E*. Generally, the Brewster angle of $\theta_{B,vac} = \arccos\sqrt{\frac{\epsilon_{r,I}\epsilon_{r,II}}{\epsilon_{r,I}+\epsilon_{r,II}}}$ at the interface between dielectrics I and II is not equal to the Brewster angle of $\theta'_{B,vac} = \arccos\sqrt{\frac{\epsilon_{r,I}\epsilon_{r,II}}{\epsilon_{r,X}+1}}$ at the interface between dielectric X (X = I or II) and vacuum, when $\epsilon_{r,X} \neq 1$. This way, there is nonzero reflection at the first and final interfaces of the designed layered nanostructure, despite that the emitted light propagates along the Brewster angle $\theta_{B,X}$ in Fig. 4*A*. Correspondingly, the value of $\mathrm{mod}(\phi_{Brew}, 2\pi)$ would be randomly distributed within the range of [0, $2\pi$) in Fig. 4*A*, namely $\mathrm{mod}(\phi_{Brew}, 2\pi) \in [0, 2\pi)$, where $\phi_{Brew}/2 = \sum_{j=2}^{N} k_{z,j}\left(Z_j - Z_{j-1}\right)$ is the accumulated phase during the propagation of light at $\theta = \theta_{B,X}$ from the first interface to the final one. Because of this random phase accumulation, the interference between multiply scattered resonance transition radiation at the forward vacuum region might be randomly constructive or destructive. As a result, Fig. 4*D* shows that the value of $U(\lambda_0, \theta_{B,vac})$ for resonance transition radiation from various Brewster randomness in Fig. 4*A* has an increasing tendency but randomly oscillates with the increasing interface number.

This random-oscillation dependence on the interface number in Fig. 4 *A* and *D* could be detrimental for practical applications. Below, two ways are proposed to eliminate this random oscillation. One way is to add an additional layer composed of dielectric X at the bottom of layered nanostructures with the Brewster randomness in Fig. 4*B*. The thickness of this additional layer does not need to fulfill Eqs. **2** and **3** but should be judiciously designed to enable $\mathrm{mod}(\phi_{Brew}, 2\pi) = 0$, where the accumulated phase now becomes $\phi_{Brew}/2 = \left[\sum_{j=2}^{N} k_{z,j}\left(Z_j - Z_{j-1}\right)\right] + k_{z,N+1}$

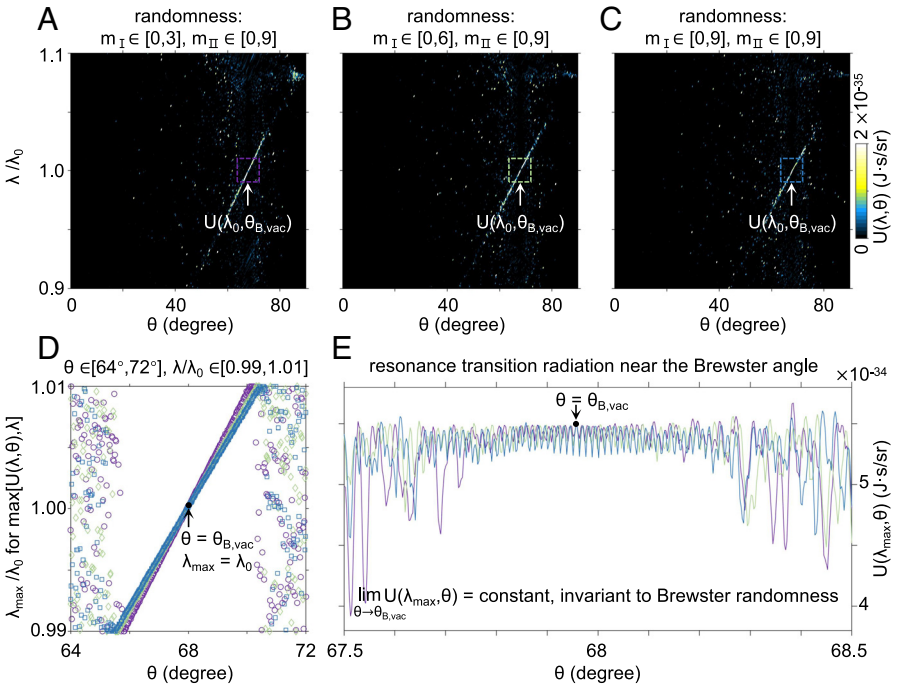


**Fig. 3.** Free-electron resonance transition radiation via Brewster randomness in the energy–momentum space. The energy–momentum space is equivalent to the $\lambda$-$\theta$ parameter space, since the working wavelength $\lambda$ and the radiation angle $\theta$ are related to the photon energy $E_{photon} = 2\pi\hbar c/\lambda$ and the component of photon momentum parallel to the interface $p_{||} = \sin\theta \bullet 2\pi\hbar/\lambda$, respectively. (*A*–*C*) Angular spectral energy density $U(\lambda, \theta)$ of free-electron forward radiation from layered aperiodic nanostructures with various Brewster randomness. For illustration, the layered aperiodic nanostructure here has $N$ = 1,000, $\varepsilon_{r,I}$ = 6.1 [e.g., $SrTiO_3$ (94)] and $\varepsilon_{r,II}$ = 1. (*D*) Dependence of $\lambda_{max}$ on $\theta$ for various Brewster randomness, as extracted from *A*–*C*. To be specific, $\lambda_{max}$ is calculated by using $U(\lambda_{max}, \theta) = \max U(\lambda, \theta), \lambda]$ inside the region of $\lambda/\lambda_0 \in [0.99, 1.01]$ and $\theta \in [64°, 72°]$, which corresponds to the region highlighted by a dashed rectangle in *A*–*C*. (*E*) Dependence of $U(\lambda_{max}, \theta)$ on $\theta$. The value of $U(\lambda_0, \theta_{B,vac})$ is a constant regardless of Brewster randomness.

$(Z_{N+1} - Z_N) = \sum_{j=2}^{N+1} k_{z,j}(Z_j - Z_{j-1})$. Under this scenario, the multiply scattered resonance transition radiation at the forward vacuum region would be all in-phase and then interfere constructively. As a result, Fig. 4*D* shows that the value of $U(\lambda_0, \theta_{B,vac})$ for resonance transition radiation from various Brewster randomness in Fig. 4*B* is proportional to $N^2$, namely $U(\lambda_0, \theta_{B,vac}) \propto N^2$, when the interface number is $N \gg 1$ (e.g., $N > 100$). Similarly, if the thickness of this additional layer is designed to have $\mathrm{mod}(\phi_{Brew}, 2\pi) = \pi$ in Fig. 4*B*, the destructive interference would always happen for these multiply scattered resonance transition radiation at the forward vacuum region. By comparing the two cases with $\mathrm{mod}(\phi_{Brew}, 2\pi) = 0$ or $\pi$ in Fig. 4 *B* and *D* further shows that when $N \gg 1$, the judicious design of this additional layer could improve the radiation intensity by one order of magnitude, which is favorable in practical applications.

The other way is to let one of the constituent dielectrics be vacuum (e.g., $\varepsilon_{r,II} = 1$) in Fig. 4*C*. This way, we have $\theta_{B,X} = \theta'_{B,X}$, and there is zero reflection at the first and final interfaces of the designed layered nanostructure in Fig. 4*C*. As a result, Fig. 4*D* shows that the case in Fig. 4*C* has $U(\lambda_0, \theta_{B,vac}) \propto N^2$ for arbitrary interface number $N$. In this case, Fig. 4*E* shows the dependence of the angular width $\Delta\theta_{FWHM}$ and the spectral width $\Delta\lambda_{FWHM}$ on the interface number, where $\Delta\theta_{FWHM}$ and $\Delta\lambda_{FWHM}$ are the full width at half maximum (FWHM) of $U(\lambda_0, \theta)$ and $U(\lambda, \theta_{B,vac})$, respectively. From Fig. 4*E*, both the angular width and the spectral width are proportional to $1/N$, namely $\Delta\lambda_{FWHM} \propto 1/N$ and $\Delta\theta_{FWHM} \propto 1/N$, if $N \gg 1$. We further show in *SI Appendix*, Fig. S9 the influence of material loss on these revealed relations (e.g., $U(\lambda_0, \theta_{B,vac}) \propto N^2$ and $\Delta\theta_{FWHM} \propto 1/N$) and find that these relations would keep almost unchanged when both the material loss and $N$ are reasonably large. This further indicates the possibility to extend the revealed phenomenon of resonance transition radiation via Brewster randomness from all-dielectric systems studied to other plasmonic and photonic systems (3, 100, 101), once the material loss is reasonably large.

## Discussion

In conclusion, we have revealed that the free-electron resonance transition radiation from layered aperiodic nanostructures could have both its intensity and directionality invariant to the long-range Brewster randomness. This invariance-to-randomness correspondence of free-electron radiation from random media might inspire disruptive ways to control light-matter interactions and facilitate the development of miniaturized optical devices driven by free electrons. For example, with the aid of optical broadband angular filter (89, 102–104), the revealed resonance transition radiation via Brewster randomness may enable the exploration of advanced light sources at some previously unreachable spectral regimes (e.g., terahertz, far-infrared, and mid-infrared), simultaneously with high directionality and narrow frequency bandwidth. If a series of layered nanostructures with the Brewster randomness are designed to work at various equally spaced frequencies and then stacked together, a more-complex layered nanostructure with multiple Brewster randomness would be formed, and its interaction with free electrons might give rise to optical frequency combs (105–108). Meanwhile, if the optical gain is introduced into the design of layered nanostructures, the resultant Brewster randomness with optical gain might be exploited for the realization of random lasers (83, 109–111). These optical devices driven by the interactions between free-electrons and the Brewster randomness could be of paramount importance to practical applications,

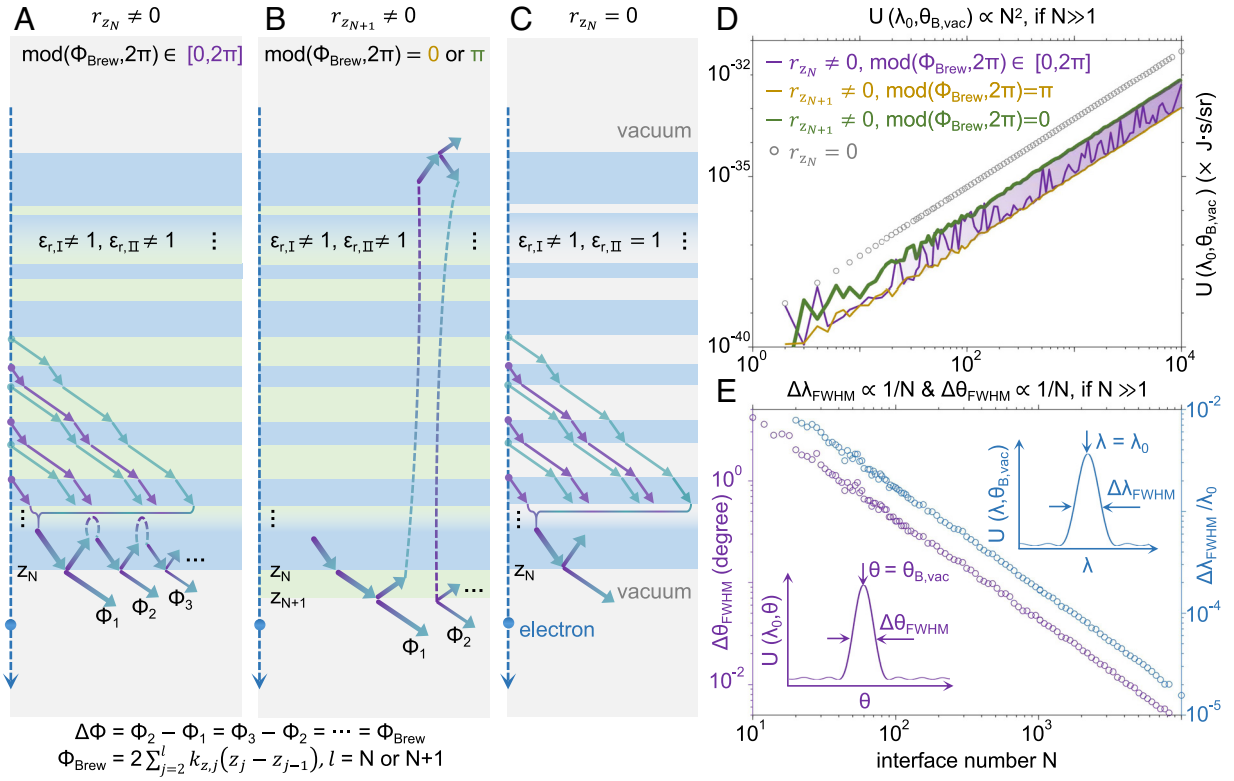


**Fig. 4.** Dependence of the intensity, angular width, and spectral width of free-electron resonance transition radiation via Brewster randomness on the interface number. (*A–C*) Structural schematic. The layered aperiodic nanostructure with Brewster randomness has $\varepsilon_{r,I} = 3.4$ [e.g., $Y_3Al_5O_{12}$ (94, 96)] in *A–C*, $\varepsilon_{r,II} = 1.4$ [e.g., $ZrO_2$ aerogel (95)] in *A* and *B* but $\varepsilon_{r,II} = 1$ in *C*. For emitted light with $\theta = \theta_{B,vac}$, there would be nonzero reflection at the first and final interfaces in *A* and *B*, since both $\varepsilon_{r,I}$ and $\varepsilon_{r,II}$ are not equal to one. As a result, $\mathrm{mod}(\phi_{Brew}, 2\pi)$ is generally randomly distributed within the range of $[0, 2\pi)$ in *A*, where $\phi_{Brew}/2$ is the accumulated phase during the propagation of light with $\theta = \theta_{B,vac}$ from the first interface to the final one. Particularly, $\mathrm{mod}(\phi_{Brew}, 2\pi) = 0$ (or $\pi$) could be achieved if an additional layer with a judiciously designed thickness is added at the bottom of the layered structure in *B*, and correspondingly, the transmitted forward radiation into region $N + 2$ could interfere constructively (or destructively). By contrast, if $\varepsilon_{r,II} = 1$, there would be zero reflection at the first and final interfaces for emitted light with $\theta = \theta_{B,vac}$ in *C*. (*D*) Dependence of the angular spectral energy density $U(\lambda_0, \theta_{B,vac})$ on the interface number *N* for cases investigated in *A–C*. (*E*) Dependence of the angular width $\Delta\theta_{FWHM}$ and the spectral width $\Delta\lambda_{FWHM}$ on *N* for the case investigated in *C*, where $\Delta\theta_{FWHM}$ and $\Delta\lambda_{FWHM}$ correspond to the full width at half maximum (FWHM) of $U(\lambda_0, \theta)$ and $U(\lambda, \theta_{B,vac})$, respectively; see *Insets*.

including on-chip information processing, communications, chemical detection, biomedical sensing, and imaging.

## Methods

**Derivation of Free-Electron Resonance Transition Radiation from Layered Aperiodic Nanostructures.** Within the framework of classical electromagnetics, Ginzburg and Frank's theory of transition radiation from a single interface in *SI Appendix*, Fig. S1 is extended to a layered aperiodic nanostructure with *N* interfaces in *SI Appendix*, Fig. S2. The angular spectral energy density and excited field distribution of free-electron radiation are analytically derived in *SI Appendix*, section S1. To be specific, the field distribution in real space can be derived by performing the plane-wave expansion, that is, $-E^R(-r,t) = \int d\omega d-k_\perp E^R_{-k_\perp,\omega} e^{j-k_\perp-r_\perp-i\omega t}$. After some calculations, the distribution of radiation field in region *j* is obtained as

$$E^R_{-k_\perp,\omega,z,j} = \begin{cases} \dfrac{iq}{\omega\varepsilon_0(2\pi)^3}\cdot a_1\cdot e^{-ik_{z,1}(z-d_1)} & (j=1) \\ \dfrac{iq}{\omega\varepsilon_0(2\pi)^3}\left[a_j^-\cdot e^{-ik_{z,j}(z-d_j)} + a_j^+\cdot e^{ik_{z,j}(z-d_{j-1})}\right] & (2\le j\le N) \\ \dfrac{iq}{\omega\varepsilon_0(2\pi)^3}\cdot a_{N+1}\cdot e^{ik_{z,N+1}(z-d_N)} & (j=N+1) \end{cases},$$

where $a_j^-$ ($a_j^+$) is the generalized factor for the backward (forward) radiation in region *j*. Based on the knowledge of the radiation field, the forward angular spectral energy density is obtained as $U(\lambda,\theta) = \frac{\varepsilon_{r,N+1}^{3/2} q^2 \cos^2\theta \left|a_{N+1}\right|^2}{4\pi^3\varepsilon_0 c \sin^2\theta}$.

**Resonance Transition Radiation via Brewster Randomness at the Brewster Angle.** The forward angular spectral energy intensity $U(\lambda_0, \theta_{B,vac})$ of resonance transition radiation via the Brewster randomness at the Brewster angle is analytically obtained in *SI Appendix*, section S2. The dependence of $U(\lambda_0, \theta_{Brew})$ on different parameters, including the interface number, the dielectric permittivities, and the electron velocity, is also analyzed.

**Influence of Short-Range Disorders on the Performance of Brewster Randomness.** More discussion on the Brewster randomness is provided in *SI Appendix*, section S3, such as the comparison for the long-range Brewster randomness and the short-range structural disorders in *SI Appendix*, Fig. S3, and the influence of short-range structural disorders on the optical features of the revealed resonance transition radiation via the Brewster randomness in *SI Appendix*, Figs. S4 and S5.

**More Discussion on the Resonance Transition Radiation via Brewster Randomness.** We provide more discussion on the resonance transition radiation via Brewster randomness in *SI Appendix*, section S4, including the destructive interference of multiple transition radiation created at adjacent interfaces in *SI Appendix*, Fig. S6, the influence of material dispersion, material loss, and interface number on the resonance transition radiation via Brewster randomness in *SI Appendix*, Figs. S7–S10, the photon yield of resonance transition radiation via Brewster randomness in *SI Appendix*, Figs. S11 and S12, and the resonance transition radiation via Brewster randomness from layered nanostructures composed of realistic materials in *SI Appendix*, Fig. S13.

**Data, Materials, and Software Availability.** The data represented in all figures are available on 10.5281/zenodo.14211143 (112). All theoretical and numerical findings can be reproduced based on the information in the article and/or *SI Appendix*.

**ACKNOWLEDGMENTS.** X.L. acknowledges the support partly from the Fundamental Research Funds for the Central Universities under Grant No. 226-2024-00022, the National Natural Science Fund for Excellent Young Scientists Fund Program (Overseas) of China, the National Natural Science Foundation of China (NSFC) under Grant No. 62475227 and No. 62175212, and Zhejiang Provincial Natural Science Fund Key Project under Grant No. LZ23F050003. H.C. acknowledges the support from the Key Research and Development Program of the Ministry of Science and Technology under Grants No. 2022YFA1404704, 2022YFA1405200, and 2022YFA1404902, the Key Research and Development Program of Zhejiang Province under Grant No.2022C01036, and the Fundamental Research Funds for the Central Universities. R.C. acknowledges the support from the NSFC under Grant No. 623B2089. Y.Y. acknowledges the support from the NSFC Excellent Young Scientists Fund (HKU 12222417), the Hong Kong Research Grant Council Strategic Topics Grant No. STG3/E-704/23-N, the startup fund of The University of Hong Kong, and an Asian Young Scientist Fellowship. B.Z. acknowledges the support from Singapore National Research Foundation Competitive Research Program No. NRF-CRP23-2019-0007.

Author affiliations: [a]Interdisciplinary Center for Quantum Information, State Key Laboratory of Extreme Photonics and Instrumentation, College of Information Science and Electronic Engineering, Zhejiang University, Hangzhou 310027, China; [b]International Joint Innovation Center, The Electromagnetics Academy at Zhejiang University, Zhejiang University, Haining 314400, China; [c]Chu Kochen Honors College, Zhejiang University, Hangzhou 310027, China; [d]Department of Physics, HK Institute of Quantum Science and Technology, The University of Hong Kong, Pokfulam, Hong Kong 999077, China; [e]Division of Physics and Applied Physics, School of Physical and Mathematical Sciences, Nanyang Technological University, Singapore 637371, Singapore; [f]Centre for Disruptive Photonic Technologies, Nanyang Technological University, Singapore 637371, Singapore; [g]Key Laboratory of Advanced Micro/Nano Electronic Devices and Smart Systems of Zhejiang, Jinhua Institute of Zhejiang University, Zhejiang University, Jinhua 321099, China; [h]Shaoxing Institute of Zhejiang University, Zhejiang University, Shaoxing 312000, China; and [i]Department of Electrical and Computer Engineering, Technion-Israel Institute of Technology, Haifa 32000, Israel

1. Y. Yang *et al.*, Free-electron interaction with nonlinear optical states in microresonators. *Science* **383**, 168–173 (2024).
2. Y. Yang *et al.*, Photonic flatband resonances for free-electron radiation. *Nature* **613**, 42–47 (2023).
3. S. Huang *et al.*, Multicolor x-rays from free electron–driven van der Waals heterostructures. *Sci. Adv.* **9**, eadj8584 (2023).
4. A. Karnieli, S. Fan, Jaynes-Cummings interaction between low-energy free electrons and cavity photons. *Sci. Adv.* **9**, eadh2425 (2023).
5. X. Gao, X. Zhao, X. Ma, T. Dong, Free electron emission in vacuum assisted by photonic time crystals. *J. Phys. D Appl. Phys.* **57**, 315112 (2024).
6. C. Roques-Carmes *et al.*, Free-electron–light interactions in nanophotonics. *Appl. Phys. Rev.* **10**, 011303 (2023).
7. Z. Su *et al.*, Manipulating Cherenkov radiation and Smith-Purcell radiation by artificial structures. *Adv. Opt. Mater.* **7**, 1801666 (2019).
8. P. A. Cherenkov, Visible emission of clean liquids by action of gamma radiation. *Dokl. Akad. Nauk SSSR* **2**, 451–454 (1934).
9. W. Galbraith, J. V. Jelley, Light pulses from the night sky associated with cosmic rays. *Nature* **171**, 349–350 (1953).
10. M. Amenomori *et al.*, First detection of photons with energy beyond 100 TeV from an astrophysical source. *Phys. Rev. Lett.* **123**, 051101 (2019).
11. R. Abbasi *et al.*, Observation of high-energy neutrinos from the Galactic plane. *Science* **380**, 1338–1343 (2023).
12. I. E. Tamm, I. M. Frank, Coherent radiation of fast electrons in a medium. *Dokl. Akad. Nauk SSSR* **14**, 107–112 (1937).
13. I. Tamm, Radiation emitted by uniformly moving electrons. *J. Phys. (USSR)* **1**, 439–454 (1939).
14. S. Xi *et al.*, Experimental verification of reversed Cherenkov radiation in left-handed metamaterial. *Phys. Rev. Lett.* **103**, 194801 (2009).
15. S. Liu *et al.*, Surface polariton Cherenkov light radiation source. *Phys. Rev. Lett.* **109**, 153902 (2012).
16. P. Genevet *et al.*, Controlled steering of Cherenkov surface plasmon wakes with a one-dimensional metamaterial. *Nat. Nanotechnol.* **10**, 804–809 (2015).
17. Z. Duan *et al.*, Observation of the reversed Cherenkov radiation. *Nat. Commun.* **8**, 14901 (2017).
18. F. Liu *et al.*, Integrated Cherenkov radiation emitter eliminating the electron velocity threshold. *Nat. Photonics* **11**, 289–292 (2017).
19. Y. Adiv *et al.*, Observation of 2D Cherenkov radiation. *Phys. Rev. X* **13**, 011002 (2023).
20. X. Guo *et al.*, Mid-infrared analogue polaritonic reversed Cherenkov radiation in natural anisotropic crystals. *Nat. Commun.* **14**, 2532 (2023).
21. Z. Gong *et al.*, Interfacial Cherenkov radiation from ultralow-energy electrons. *Proc. Natl. Acad. Sci. U.S.A.* **120**, e2306601120 (2023).
22. Z. Xu *et al.*, Observation of analog flatland Cherenkov radiations on metasurfaces. *Laser. Photon. Rev.* **18**, 2300763 (2024).
23. V. L. Ginzburg, I. M. Frank, Radiation of a uniformly moving electron due to its transition from one medium into another. *J. Phys. (USSR)* **9**, 353–362 (1945).
24. P. Goldsmith, J. V. Jelley, Optical transition radiation from protons entering metal surfaces. *Philos. Mag.* **4**, 836–844 (1959).
25. V. L. Ginzburg, *Transition Radiation and Transition Scattering* (A. Hilger, 1990).
26. S. N. Galyamin, A. V. Tyukhtin, A. Kanareykin, P. Schoessow, Reversed Cherenkov-transition radiation by a charge crossing a left-handed medium boundary. *Phys. Rev. Lett.* **103**, 194802 (2009).
27. I. P. Ivanov, D. V. Karlovets, Detecting transition radiation from a magnetic moment. *Phys. Rev. Lett.* **110**, 264801 (2013).
28. X. Lin *et al.*, Controlling Cherenkov angles with resonance transition radiation. *Nat. Phys.* **14**, 816–821 (2018).
29. Y. Yu *et al.*, Transition radiation in photonic topological crystals: Quasiresonant excitation of robust edge states by a moving charge. *Phys. Rev. Lett.* **123**, 057402 (2019).
30. R. Chen *et al.*, Free-electron Brewster-transition radiation. *Sci. Adv.* **9**, eadh8098 (2023).
31. J. Chen *et al.*, Low-velocity-favored transition radiation. *Phys. Rev. Lett.* **131**, 113002 (2023).
32. R. Chen *et al.*, Recent advances of transition radiation: Fundamentals and applications. *Mater. Today Electron.* **3**, 100025 (2023).
33. G. B. Yodh, X. Artru, R. Ramaty, Transition radiation in astrophysics. *Astrophys. J.* **181**, 725–736 (1973).
34. K. Y. Platonov, G. D. Fleishman, Transition radiation in media with random inhomogeneities. *Phys. Uspekhi* **45**, 235 (2002).
35. A. Feist *et al.*, Quantum coherent optical phase modulation in an ultrafast transmission electron microscope. *Nature* **521**, 200–203 (2015).
36. K. Wang *et al.*, Coherent interaction between free electrons and a photonic cavity. *Nature* **582**, 50–54 (2020).
37. D. Pan, H. Xu, Polarizing free electrons in optical near fields. *Phys. Rev. Lett.* **130**, 186901 (2023).
38. M. Yannai *et al.*, Lossless monochromator in an ultrafast electron microscope using near-field THz radiation. *Phys. Rev. Lett.* **131**, 145002 (2023).
39. Y. Auad *et al.*, μeV electron spectromicroscopy using free-space light. *Nat. Commun.* **14**, 4442 (2023).
40. T. Bucher *et al.*, Free-electron Ramsey-type interferometry for enhanced amplitude and phase imaging of nearfields. *Sci. Adv.* **9**, eadi5729 (2023).
41. P. G. O'Shea, H. P. Freund, Free-electron lasers: Status and applications. *Science* **292**, 1853–1858 (2001).
42. G. Perosa *et al.*, Femtosecond polarization shaping of free-electron laser pulses. *Phys. Rev. Lett.* **131**, 045001 (2023).
43. E. Prat *et al.*, An X-ray free-electron laser with a highly configurable undulator and integrated chicanes for tailored pulse properties. *Nat. Commun.* **14**, 5069 (2023).
44. O. Chamberlain, E. Segrè, C. Wiegand, T. Ypsilantis, Observation of antiprotons. *Phys. Rev.* **100**, 947 (1955).
45. J. J. Aubert *et al.*, Experimental observation of a heavy particle. *J. Phys. Rev. Lett.* **33**, 1404 (1974).
46. P. Bagnaia *et al.*; UA2 Collaboration, Evidence for Z0→ e+ e− at the CERN pp collider. *Phys. Lett. B* **129**, 130–140 (1983).
47. F. Reines, The neutrino: From poltergeist to particle. *Rev. Mod. Phys.* **68**, 317 (1996).
48. ATLAS Collaboration, Observation of a new particle in the search for the Standard Model Higgs boson with the ATLAS detector at the LHC. *Phys. Lett. B* **716**, 1–29 (2012).
49. H. Hu *et al.*, Surface Dyakonov-Cherenkov radiation. *eLight* **2**, 2 (2022).
50. L. Wartski, J. Marcou, S. Roland, Detection of optical transition radiation and its application to beam diagnostics. *IEEE Trans. Nucl. Sci.* **20**, 544–548 (1973).
51. H. Liu *et al.*, Cherenkov radiation-based optical fibre diagnostics of fast electrons generated in intense laser-plasma interactions. *Rev. Sci. Instruments* **89**, 083302 (2018).
52. J. Sloan, N. Rivera, J. D. Joannopoulos, M. Soljačić, Controlling two-photon emission from superluminal and accelerating index perturbations. *Nat. Phys.* **18**, 67–74 (2022).
53. A. K. Glaser, R. Zhang, D. J. Gladstone, B. W. Pogue, Optical dosimetry of radiotherapy beams using Cherenkov radiation: The relationship between light emission and dose. *Phys. Med. Biol.* **59**, 3789 (2014).
54. X. Cui *et al.*, Beyond external light: On-spot light generation or light delivery for highly penetrated photodynamic therapy. *ACS Nano* **17**, 20776–20803 (2023).
55. S. John, Electromagnetic absorption in a disordered medium near a photon mobility edge. *Phys. Rev. Lett.* **53**, 2169 (1984).
56. M. Segev, Y. Silberberg, D. N. Christodoulides, Anderson localization of light. *Nat. Photonics* **7**, 197–204 (2013).
57. A. Yamilov *et al.*, Anderson localization of electromagnetic waves in three dimensions. *Nat. Phys.* **19**, 1308–1313 (2023).
58. P. W. Anderson, Absence of diffusion in certain random lattices. *Phys. Rev.* **109**, 1492 (1958).
59. N. W. Ashcroft, N. D. Mermin, *Solid State Physics* (Harcourt College, 1976).
60. J. Ruze, Antenna tolerance theory–A review. *Proc. IEEE* **54**, 633–640 (1966).
61. S. P. Kapitsa, Radiation from a charge moving in an inhomogeneous medium. *J. Exp. Theor. Phys.* **39**, 1367 (1960).
62. V. V. Tamoykin, Cherenkov and transient radiation of uniformly moving charge in random inhomogeneous medium. *Astrophys. Space Sci.* **16**, 120–129 (1972).
63. K. Y. Platonov, I. Toptygin, G. D. FleÄshman, Emission of radiation by particles in media with inhomogeneities and coherent bremsstrahlung. *Soviet Phys. Uspekhi* **33**, 289 (1990).
64. A. I. Alikhanian, K. M. Avakina, G. M. Garibian, M. P. Lorikian, K. K. Shikhliarov, Detection of X-Ray transition radiation by means of a spark chamber. *Phys. Rev. Lett.* **25**, 635 (1970).
65. Z. S. Gevorkian, Smith-Purcell radiation from rough surfaces. *Phys. Rev. ST Accel. Beams* **13**, 070705 (2010).
66. F. J. G. de Abajo, Optical excitations in electron microscopy. *Rev. Mod. Phys.* **82**, 209 (2010).
67. X. Shi, L. W. W. Wong, S. Huang, L. J. Wong, I. Kaminer, Transverse recoil imprinted on free-electron radiation. *Nat. Commun.* **15**, 7803 (2024).
68. S. Huang *et al.*, Quantum recoil in free-electron interactions with atomic lattices. *Nat. Photonics* **17**, 224–230 (2023).
69. R. Dahan *et al.*, Creation of optical cat and GKP states using shaped free electrons. *Phys. Rev. X* **13**, 031001 (2023).
70. F. J. G. de Abajo, E. J. C. Dias, V. Di Giulio, Complete excitation of discrete quantum systems by single free electrons. *Phys. Rev. Lett.* **129**, 093401 (2022).

71. A. Feist *et al.*, Cavity-mediated electron-photon pairs. *Science* **377**, 777–780 (2022).
72. F. J. G. de Abajo, C. Ropers, Spatiotemporal electron beam focusing through parallel interactions with shaped optical fields. *Phys. Rev. Lett.* **130**, 246901 (2023).
73. S. Zhu *et al.*, Harnessing disordered photonics via multi-task learning towards intelligent four-dimensional light field sensors. *PhotoniX* **4**, 26 (2023).
74. Y. Liu *et al.*, Three-channel robust optical encryption via engineering coherence Stokes vector of partially coherent light. *PhotoniX* **5**, 8 (2024).
75. C. Wang *et al.*, Superscattering of light: Fundamentals and applications. *Rep. Progress Phys.* **87**, 126401 (2024).
76. J. R. M. Saavedra, D. Castells-Graells, F. J. G. de Abajo, Smith–Purcell radiation emission in aperiodic arrays. *Phys. Rev. B* **94**, 035418 (2016).
77. R. Remez *et al.*, Spectral and spatial shaping of Smith–Purcell radiation. *Phys. Rev. A* **96**, 061801 (2017).
78. I. Kaminer *et al.*, Spectrally and spatially resolved Smith–Purcell radiation in plasmonic crystals with short-range disorder. *Phys. Rev. X* **7**, 011003 (2017).
79. F. Chen *et al.*, Tuning Smith–Purcell radiation by rotating a metallic nanodisk array. *Opt. Lett.* **48**, 2002–2005 (2023).
80. Z. Zhang *et al.*, Chiral plasmons enable coherent vortex Smith–Purcell radiation. *Laser. Photon. Rev.* **17**, 2200420 (2023).
81. Z. Su, F. Cheng, L. Li, Y. Liu, Complete control of Smith–Purcell radiation by graphene metasurfaces. *ACS Photonics* **6**, 1947–1954 (2019).
82. Z. Wang, K. Yao, M. Chen, H. Chen, Y. Liu, Manipulating Smith–Purcell emission with babinet metasurfaces. *Phys. Rev. Lett.* **117**, 157401 (2016).
83. R. Sapienza, Controlling random lasing action. *Nat. Phys.* **18**, 976–979 (2022).
84. M. N. Bera, A. Acín, M. Kuś, M. W. Mitchell, M. Lewenstein, Randomness in quantum mechanics: Philosophy, physics and technology. *Rep. Progress Phys.* **80**, 124001 (2017).
85. K. Kim *et al.*, Massively parallel ultrafast random bit generation with a chip-scale laser. *Science* **371**, 948–952 (2021).
86. D. Brewster, On the laws which regulate the polarization of light by reflection from transparent bodies. *Philos. Trans. R. Soc. Lond.* **105**, 125–159 (1815).
87. J. E. Sipe, P. Sheng, B. S. White, M. H. Cohen, Brewster anomalies: A polarization-induced delocalization effect. *Phys. Rev. Lett.* **60**, 108 (1988).
88. Z. Wu, F. Zhai, F. M. Peeters, H. Q. Xu, K. Chang, Valley-dependent Brewster angles and Goos-Hänchen effect in strained graphene. *Phys. Rev. Lett.* **106**, 176802 (2011).
89. Y. Shen *et al.*, Optical broadband angular selectivity. *Science* **343**, 1499–1501 (2014).
90. R. Paniagua-Domínguez *et al.*, Generalized Brewster effect in dielectric metasurfaces. *Nat. Commun.* **7**, 10362 (2016).
91. X. Lin, Y. Shen, I. Kaminer, H. Chen, M. Soljačić, Transverse-electric Brewster effect enabled by nonmagnetic two-dimensional materials. *Phys. Rev. A* **94**, 023836 (2016).
92. Z. Chen *et al.*, Graphene controlled Brewster angle device for ultra broadband terahertz modulation. *Nat. Commun.* **9**, 4909 (2018).
93. X. Lin *et al.*, A Brewster route to Cherenkov detectors. *Nat. Commun.* **12**, 5554 (2021).
94. E. D. Palik, *Handbook of Optical Constants of Solids* (Academic press, 1998).
95. A. Pirvaram, N. Talebzadeh, M. Rostami, S. N. Leung, P. G. O'Brien, Evaluation of a ZrO2/ZrO2-aerogel one-dimensional photonic crystal as an optical filter for thermophotovoltaic applications. *Thermal Sci. Eng. Progress* **25**, 100968 (2021).
96. J. Hrabovský, M. Kučera, L. Paloušová, L. Bi, M. Veis, Optical characterization of Y3Al5O12 and Lu3Al5O12 single crystals. *Opt. Mater. Express* **11**, 1218–1223 (2021).
97. K. Leosson, B. Agnarsson, Integrated biophotonics with CYTOP. *Micromachines* **3**, 114–125 (2012).
98. G. Adamo *et al.*, Light well: A tunable free-electron light source on a chip. *Phys. Rev. Lett.* **103**, 113901 (2009).
99. Z. Dang *et al.*, Chiral Smith-Purcell radiation light source. *Adv. Opt. Mater.* **11**, 2300274 (2023).
100. H. Hu *et al.*, Nonlocality induced Cherenkov threshold. *Laser. Photon. Rev.* **14**, 2000149 (2020).
101. H. Hu *et al.*, Broadband enhancement of Cherenkov radiation using dispersionless plasmons. *Adv. Sci.* **9**, 2200538 (2022).
102. Y. Shen *et al.*, Metamaterial broadband angular selectivity. *Phys. Rev. B* **90**, 125422 (2014).
103. Y. Shen, C. W. Hsu, Y. X. Yeng, J. D. Joannopoulos, M. Soljačić, Broadband angular selectivity of light at the nanoscale: Progress, applications, and outlook. *Appl. Phys. Rev.* **3**, 011103 (2016).
104. Y. Qu *et al.*, Polarization–independent optical broadband angular selectivity. *ACS Photonics* **5**, 4125–4131 (2018).
105. V. Brasch *et al.*, Photonic chip-based optical frequency comb using soliton Cherenkov radiation. *Science* **351**, 357–360 (2016).
106. N. Picqué, T. W. Hänsch, Frequency comb spectroscopy. *Nat. Photonics* **13**, 146–157 (2019).
107. S. A. Diddams, K. Vahala, T. Udem, Optical frequency combs: Coherently uniting the electromagnetic spectrum. *Science* **369**, eaay3676 (2020).
108. L. Chang, S. Liu, J. E. Bowers, Integrated optical frequency comb technologies. *Nat. Photonics* **16**, 95–108 (2022).
109. D. S. Wiersma, The physics and applications of random lasers. *Nat. Phys.* **4**, 359–367 (2008).
110. N. Bachelard, J. Andreasen, S. Gigan, P. Sebbah, Taming random lasers through active spatial control of the pump. *Phys. Rev. Lett.* **109**, 033903 (2012).
111. H. Cao, R. Chriki, S. Bittner, A. A. Friesem, N. Davidson, Complex lasers with controllable coherence. *Nat. Rev. Phys.* **1**, 156–168 (2019).
112. Z. Gong, Free-electron resonance transition radiation via brewster randomness–Data set [Data set]. Zenodo. (2024). https://doi.org/10.5281/zenodo.14211143. Deposited 24 November 2024.